Acta Crystallographica Section D
Biological Crystallography
ISSN 0907-4449

Structure of a constitutively activated RhoA mutant (Q63L) at 1.55 Å resolution

Kenton Longenecker,† Paul Read, Shin-Kai Lin, Andrew P. Somlyo, Robert K. Nakamoto and Zygmunt S. Derewenda*

Department of Molecular Physiology and Biological Physics, University of Virginia, Charlottesville, VA 22908, USA

† Present address: Department of Structural Biology, Abbott Laboratories, Abbott Park, IL 60064, USA.

Correspondence e-mail: zsd4n@avery.med.virginia.edu

Received 16 September 2002
Accepted 6 March 2003

PDB Reference: Q63L RhoA mutant, 1kmq, r1kmqsf.

Mutants of the small G protein RhoA that are deficient in GTPase activity and thereby exhibit constitutive molecular signaling activity are commonly used to discover its cellular functions. In particular, two such mutants, Gly14→Val (G14V) and Gln63→Leu (Q63L), are often used interchangeably for such studies. However, while their *in vitro* rates of GTP hydrolysis are very similar, differences are observed in their other functional properties. The structure of G14V-RhoA is known; in order to assess whether structural variations are responsible for functional differences, the crystal structure of a Q63L-RhoA bound to the GTP-analog 5′-guanylylimidodiphosphate (GMPPNP) was determined at 1.5 Å resolution. Overall, the structure is very similar to that of G14V-RhoA, but the significantly higher resolution data permit an improved basis for structural analysis and comparison. The data support the notion that differences observed between the mutants *in vivo* are likely to arise from altered affinities for RhoGDI and not from direct structural differences.

1. Introduction

RhoA participates in regulatory signaling pathways and belongs to the Ras-homology family that includes Rac and Cdc42 (Hall, 1998), post-translationally prenylated GTPases which exhibit overlapping and distinct functions within the cell (Somlyo & Somlyo, 2000; Zohn *et al.*, 1998). Like other members of the Ras superfamily, Rho proteins cycle between a biologically active GTP-bound state and an inactive GDP-bound state. The cycle is tightly regulated by accessory proteins: guanine nucleotide-exchange factors (GEFs) catalyze GTP uploading and biological activation, GTPase-activating proteins (GAPs) accelerate nucleotide hydrolysis, downregulating the biological activity, and the Rho-specific guanine nucleotide-dissociation inhibitor (RhoGDI) extracts Rho proteins from the membrane by forming a cytosolic complex, solubilizes them by sequestering the prenyl moiety and stabilizes the GDP-bound form. Both membrane localization and association with RhoGDI depend upon post-translational prenylation at the C-terminus of RhoA. Structural differences between the two nucleotide-bound states are apparent upon comparison of the crystal structures of RhoA in the GDP-bound form (Wei *et al.*, 1997) and of the constitutively active G14V-RhoA mutant bound to the GTP analog GTPγS (Ihara *et al.*, 1998). Conformational changes are localized to two regions known as switch 1 (residues 28–44) and switch 2 (residues 61–69) in analogy to Ras.

Over the past decade, the biological functions of small GTPases have often been probed using constitutively active mutants which maintain the biologically active state because

© 2003 International Union of Crystallography
Printed in Denmark – all rights reserved

their intrinsic hydrolytic properties and susceptibility to downregulation by GAPs are compromised. These mutants are normally based on analogous mutants of Ras (Krengel *et al.*, 1990). In the case of RhoA, the activating point mutations G14V and Q63L of RhoA are often employed. Both sites are located in the nucleotide-binding pocket and each mutation interferes with the hydrolysis of the γ-phosphate of GTP, rendering the protein constitutively active. These two mutants are often used interchangeably, but some studies have reported functional differences. For example, a morphological difference was observed in transformed rat fibroblasts transfected with Q63L-RhoA compared with the G14V mutant (Mayer *et al.*, 1999). Another study of mammalian cells addressed differential subcellular localization of the mutants and a difference was noted in their ability to bind RhoGDI (Michaelson *et al.*, 2001). Consistent with these observations, G14V-RhoA is readily isolated in a stable protein complex with RhoGDI when they are coexpressed in yeast (Read *et al.*, 2000). In this paper, we report comparable experiments which show that the Q63L mutant yields strikingly less protein complex with RhoGDI. In an effort to rationalize such differences from a structural perspective, we determined the crystal structure of the Q63L mutant of RhoA bound to the GTP analog GMPPNP. We report its close similarity to the structure of G14V-RhoA–GTPγS at 2.4 Å resolution (Ihara *et al.*, 1998) and we postulate that the biological differences observed between the mutants are the result of rather subtle changes involving altered affinities for the accessory protein RhoGDI.

2. Materials and methods

2.1. Recombinant coexpression of RhoA and RhoGDI in yeast

The coexpression and purification of Rho proteins and RhoGDI in yeast were prepared as described previously (Read & Nakamoto, 2000). Briefly, the yeast strain SY1 was co-transformed with two plasmids, one for expression of the His_6-tagged RhoA protein and the second for expression of (FLAG)RhoGDI. Heterologous protein expression was induced in 18 l cultures by the addition of 2% galactose when $OD_{650\,nm}$ reached 1.2. Following incubation for another 8 h, cells were harvested by centrifugation and lysed. The (His_6)RhoA–(FLAG)RhoGDI complexes were purified from the soluble cytosolic portion using Ni–NTA–agarose (Qiagen) followed by M2 anti-FLAG antibody (Sigma Chemicals) chromatography.

2.2. Analysis of nucleotide content and GTP hydrolysis

Protein-bound nucleotide content and GTP-hydrolysis rates were quantified as described elsewhere (Read & Nakamoto, 2000). Briefly, protein samples were precipitated with perchloric acid and sodium acetate, releasing the nucleotide. After centrifugation, the supernatant was analyzed by isopycnic high-performance liquid chromatography (HPLC; Waters 8PSAX-10µ), monitoring the absorbance at 254 nm of the elution with 0.7 *M* ammonium phosphate pH 4.0 and quantifying peaks by comparison with standards for GDP, GTP and GTPγS. To measure GTPase activity, the bound nucleotide of protein samples was exchanged with GTP and the nucleotide content was determined by HPLC. Rate constants were determined at 295 K by fitting data to a single exponential function.

2.3. Bacterial expression and sample preparation for crystallographic studies

Point mutations to a modified pET vector (Sheffield *et al.*, 1999) encoding human RhoA were introduced using the Quickchange (Stratagene) mutagenesis procedure, separately creating expression constructs for the G14V and Q63L mutants. These constructs encode a His-tag fusion with a rTEV protease cleavage site, followed by the cloning artefact GAMGSP and the sequence of RhoA. The sequence also contains the mutations F25N, known to stabilize RhoA in bacteria, and a truncated C-terminus at residue 181. The fusion protein was expressed in BL21(DE3) *Escherichia coli* cultured in Luria broth, inducing log-phase expression with 0.5 m*M* isopropyl-β-D-thiogalactopyranoside (IPTG) and incubating for 3 h at 310 K. Pelleted cells were resuspended in homogenization buffer (50 m*M* Tris–HCl pH 8.0, 400 m*M* NaCl, 1 m*M* $MgCl_2$, 50 µ*M* GDP, 5 m*M* imidazole and 1 m*M* lysozyme) and lysed by sonication. The soluble portion was bound to Ni–NTA–agarose (Qiagen) and recovered with elution buffer (50 m*M* Tris–HCl pH 8.0, 250 m*M* NaCl, 5 m*M* $MgCl_2$, 75 µ*M* GDP, 150 m*M* imidazole).

Purified protein was digested with rTEV protease (Life Technologies) in cleavage buffer (25 m*M* Tris–HCl, 5 m*M* $MgCl_2$, 10 m*M* β-mercaptoethanol, 20 µ*M* GDP). Bound nucleotide was exchanged in a buffer with a low concentration of Mg^{2+} (50 m*M* Tris–HCl pH 8.0, 10 m*M* β-mercaptoethanol, 5 m*M* $MgCl_2$ and 10 m*M* EDTA) and incubated with the addition of 10 m*M* GMPPNP (Sigma Chemicals). After 1 h, 10 m*M* $MgCl_2$ was added and the protein was equilibrated with a final buffer (25 m*M* Tris–HCl pH 8.0, 5 m*M* $MgCl_2$, 10 m*M* β-mercaptoethanol and 2 m*M* GMPPNP). Crystals were grown by vapor diffusion, equilibrating equal volumes of protein (8 mg ml^{-1}) and reservoir solution (21% PEG 8000, 100 m*M* HEPES pH 6.9 and 20% dioxane) at 277 K.

2.4. X-ray data collection and structure determination

X-ray diffraction data were collected at NSLS beamline X9B using a Quantum CCD detector (ADSC). Intensity data were processed using *HKL*2000 (Otwinowski & Minor, 1997) and converted to structure-factor magnitudes using the *TRUNCATE* procedure within the *CCP*4 program suite (Collaborative Computational Project, Number 4, 1994). The structure was solved by molecular replacement using the program *AMoRe* (Collaborative Computational Project, Number 4, 1994) and a search model consisting of RhoA coordinates (PDB code 1ftn) without the nucleotide or the residues of the switch regions. The structure was rebuilt using *ARP*/*wARP* (Perrakis *et al.*, 2001) and finished with graphical manipulation using *O* (Jones *et al.*, 1991) and *REFMAC*5

Table 1
Purification of recombinant RhoA-RhoGDI coexpressed in yeast.

Complex	Yield (μg)	Yield (μg per g of cytosol)	Yield (% of wt yield)	GDP-bound (%)	GTP-bound (%)
(His_6)RhoA–(FLAG)RhoGDI	4500	1785	100	100	0
V14 (His_6)RhoA–(FLAG)RhoGDI	3100	1360	76	95	5
L63 (His_6)RhoA–(FLAG)RhoGDI	170	150	8	95	5

Table 2
Data-collection and refinement statistics.

Values in parentheses are values for the highest resolution shell (1.61–1.55 Å).

X-ray data	
Resolution, d_{min} (Å)	1.55
Observations	154149
Unique reflections	30966
Completeness (%)	97 (85)
$I/\sigma(I)$	18.9 (5.4)
R_{sym}† (%)	3.6 (28)
Structure refinement	
R_{cryst}/R_{free}‡ (%)	16.1/19.0
R.m.s.d. bonds (Å)	0.006
R.m.s.d. angles (°)	2.3
Mean B value (Å^2)	20.9
Protein/solvent (Å^2)	20.7/29.6

† $R_{sym} = \sum|I - \langle I\rangle|/\sum I$, where I is the integrated intensity for a reflection. ‡ R_{free} is the standard crystallographic R factor, R_{cryst}, but calculated on 5% of the data excluded from the refinement.

(Murshudov *et al.*, 1997) refinement. Figures were produced using *BOBSCRIPT* (Esnouf, 1997).

3. Results and discussion

3.1. Nucleotide status of recombinant RhoA–RhoGDI co-expressed in yeast

Purified samples of RhoA or constitutively active point mutants (G14V or Q63L) were prepared from yeast cultures, utilizing in each case a His_6 tag on the RhoA constructs and a FLAG tag on RhoGDI for an efficient two-step purification procedure from the cytosol. The total amount of (His_6)RhoA–(FLAG)RhoGDI protein complex obtained was 4.5 mg (Table 1), which equals the yield we consistently observed in multiple preparations of the complex with the tags reversed [*i.e.* (FLAG)RhoA–(His_6)RhoGDI] (Read *et al.*, 2000). Coexpression of the G14V-RhoA mutant with RhoGDI yielded slightly less purified complex than the wild type, both in terms of total protein and the normalized yield relative to the total amount of cytosolic protein, but the corresponding experiment with the Q63L-RhoA mutant yielded dramatically less complex with RhoGDI (Table 1).

The large differences between the yields for the two mutants cannot be explained by simple differences in protein expression, but suggest possible differences in nucleotide status. Therefore, the nucleotide content for each of the samples was measured (Table 1), yielding in each case a 1:1 molar ratio of bound nucleotide to protein complex. While the wild-type complex only contained GDP (*i.e.* no detectable GTP), both of the constitutively active mutants in complex with RhoGDI contained a mixture of 95% GDP and 5% GTP, consistent with our previous observations of the nucleotide status of purified complexes with RhoGDI, but with the reversed tags (Read *et al.*, 2000). However, the nucleotide content of samples purified by metal affinity alone (*i.e.* not purified by antibody column) yielded a mixture of 55% GDP and 45% GTP for the G14V sample, compared with only 8% GDP and 92% GTP for the Q63L sample. These samples would include molecules of (His_6)RhoA not bound to RhoGDI and thus the percentages represent the overall nucleotide status of the recombinant GTPase in the cytosol. Such functional differences probably underlie the phenotypic differences observed in some studies of these mutants in other physiological models.

3.2. GTPase activity of RhoA mutants expressed in bacteria

Because of the apparent differences between the G14V-RhoA and the Q63L mutants, we measured the intrinsic rates of GTP hydrolysis exhibited by mutants expressed in bacterial cells and purified by Ni^{2+}-affinity chromatography. The rate constant of GTP hydrolysis for G14V-RhoA is $3.8 \times 10^{-6}\ s^{-1}$ and that for Q63L-RhoA is $5.1 \times 10^{-6}\ s^{-1}$. For comparison, the rate constant of a matching construct with wild-type residues at positions 14 and 63 was measured as $100 \times 10^{-6}\ s^{-1}$, which is very similar to our previously reported measurement for wild-type RhoA (Read *et al.*, 2000). Thus, the two mutants hydrolyze GTP much more slowly than wild-type RhoA and under these conditions they actually have very similar rates of hydrolysis.

3.3. Structure of Q63L-RhoA bound to GMPPNP

To examine possible structural differences between the constitutively active mutants, we determined the crystal structure of Q63L-RhoA for comparison with the known crystal structure of the G14V mutant. The nucleotide bound to the purified recombinant protein was exchanged *in vitro* with the GTP analog GMPPNP. Plate-like crystals grew under conditions similar to those reported for the G14V-RhoA mutant (Ihara *et al.*, 1998), with a dramatic change from small crystalline spherulites to larger plates dependent upon increasing dioxane concentration (from 10–20%). Conveniently, dioxane also permitted a simple freezing protocol directly from the reservoir solution. X-ray data were collected from one crystal to 1.55 Å (Table 2), displaying orthorhombic $P2_12_12$ symmetry with an estimated mosaicity of 0.74° and a Wilson B factor of 16.6 Å^2. The unit cell (a = 63.58, b = 73.34, c = 48.04 Å) contains one molecule of RhoA in the asymmetric unit and 54% solvent (V_M coefficient of 2.7 Å^3 Da^{-1}).

The structure was readily determined by molecular replacement using the coordinates of RhoA (PDB code 1ftn). Starting from this model without the switch 1 and 2 regions, the electron-density maps were not biased for a GTP-bound conformation. The refined model contains residues 4–180, the GMPPNP nucleotide and an associated Mg^{2+} ion (Fig. 1). Initial difference maps clearly revealed the triphosphate

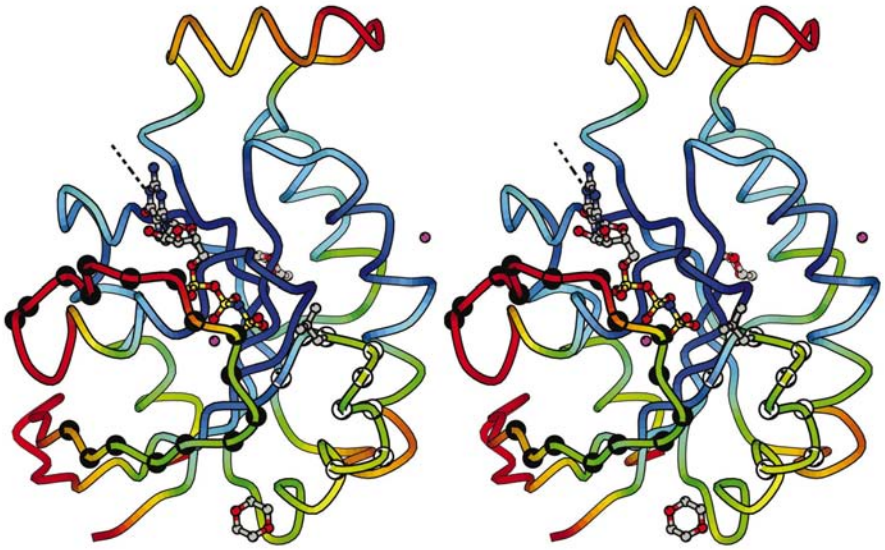

Figure 1
Stereoview of the Q63L-RhoA structure. The trace of the main chain is colored according to *B* factor, ranging from $\leq$10 Å^2 (blue) to $\geq$30 Å^2 (red). The GMPPNP molecule is displayed together with the associated Mg^{2+} ion and residues in the switch regions are highlighted by C^{α} spheres (black for switch 1 and white for switch 2). The location of two dioxane molecules and a secondary Mg^{2+} ion are also shown.

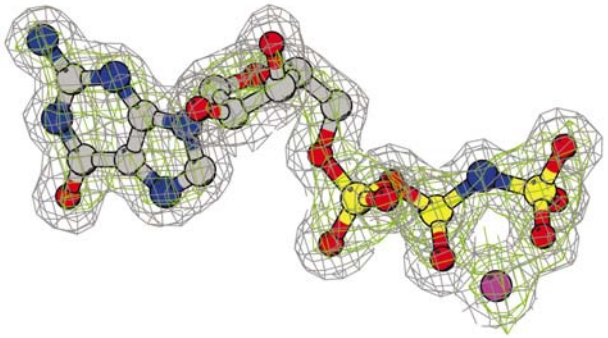

Figure 2
Electron-density maps for the GMPPNP nucleotide. The refined structure is displayed together with the final $2F_o - F_c$ electron-density map (gray) contoured at 1σ. Also shown is a $F_o - F_c$ difference map (green) contoured at 3σ using phases based on an initial model lacking the nucleotide.

features of the bound GMPPNP (Fig. 2), which is in contrast to our earlier unsuccessful structure determination of wild-type RhoA with GMPPNP, apparently hydrolyzed at the γ-phosphate as noted in a similar experiment with Cdc42 (Rudolph *et al.*, 1999). Additionally, a second Mg^{2+} ion was identified in the electron-density maps located at an intermolecular lattice contact and distinguishable from solvent based on the octahedral geometry of the interacting ligands (Asn94, Glu97 and four bridging water molecules). The high-resolution maps also revealed two dioxane molecules included in the model, suggesting a direct means by which dioxane might influence crystallization. Interestingly, one dioxane molecule is located between the switch 1 and switch 2 regions and possibly stabilizes the conformation by packing between Phe39 and Leu72, while the second dioxane molecule is found in a cleft on the opposite face of the protein. Statistics for the refined model are provided in Table 2 and represent values following the refinement of individual atomic anisotropic displacement parameters (ADP), for which the observations to refined parameter ratio was 1.9. Prior to ADP refinement, the model had a crystallographic *R* factor of 17.6% and an $R_{\rm free}$ of 20.0%.

Overall, the structure is very similar to the G14V-RhoA–GTPγS structure (PDB code 1a2b), which was determined at a resolution of 2.4 Å in the same crystal lattice. Superposition of the C^{α} atoms yields an r.m.s. deviation of 0.42 Å. The switch regions also adopt nearly identical conformations in the two structures, reminiscent of the activated forms of Rac (Hirshberg *et al.*, 1997) and Cdc42 (Nassar *et al.*, 1998). The mutated Leu63 occupies the same position as the native Gln63 residue in the G14V-RhoA structure and the atoms of the native Gly14 residue are within the expected positional error of the corresponding atoms for the G14V-RhoA mutant. The atoms of GMPPNP also overlap very closely with the positions of corresponding atoms of the GTPγS structure. Importantly, at 1.55 Å resolution, ordered solvent and atomic *B*-factor values are more accurately determined than at 2.4 Å resolution. A visual representation of the *B*-factor variation throughout the structure is highlighted in Fig. 1, which emphasizes the mobility of certain loops on the surface, notably including the N-terminal portion of switch 1 and the insert helix (residues 124–136) characteristic of the Rho family. Moreover, TLS refinement (Winn *et al.*, 2001) of the bound GMPPNP molecule suggests libration about an axis parallel to the plane of the guanine ring (Fig. 1). In contrast to negligible values for elements of the **T** and **S** tensors, the elements of the **L** tensor (m_{11} = 6.8, m_{22} = −0.7 and m_{33} = 1.0) with respect to the libration axes represent a significant correlated motion not found for the protein as a whole. These subtle features contribute to a detailed understanding of RhoA with possible implications for its functional interactions with other proteins.

The closely related structures of RhoA, Cdc42 and Rac bound to RhoGDI exhibit a binding mode for a GDP-bound conformation that is incompatible with the structures of Rho proteins in the active GTP-bound conformation (Longenecker *et al.*, 1999; Hoffman *et al.*, 2000; Scheffzek *et al.*, 2000). Interestingly, however, we observed a small but measurable fraction (5%) of GTP-bound protein for both of the RhoA mutants purified in complex with RhoGDI, a finding consistent with our previously reported experiments on G14V-RhoA (Read *et al.*, 2000). Like the G14V-RhoA structure, the conformation of Q63L-RhoA–GMPPNP is not

compatible with the observed modes of RhoGDI binding. Clearly, RhoGDI has a higher affinity for the GDP-bound form of RhoA and perhaps a compatible conformation is adopted even in the presence of a GTP analog, as exhibited in the structure of the arfaptin–Rac1–GMPPNP complex (Tarricone *et al.*, 2001).

The close similarity of the structural and biochemical features of the G14V and Q63L mutants suggests that *in vivo* differences arise from effects not evident in these studies. We note that the crystallized protein mutants are truncated constructs lacking the C-terminus, which possibly plays a differential role in the two cases. It is likely that physiological differences between the constitutive mutants arise from different *in vivo* GTPase activities for, as we report, L63-RhoA contains a greater overall GTP/GDP ratio in yeast than V14-RhoA. Thus, the L63-RhoA mutant would have lower affinity for RhoGDI and appear to function as a more active constitutive mutant than V14-RhoA.

We thank Dr Zbigniew Dauter for assistance at the NSLS, Brookhaven National Laboratory. This work was funded by NIH program project grant HL48807.

References

Collaborative Computational Project, Number 4 (1994). *Acta Cryst.* D**50**, 760–763.
Esnouf, R. M. (1997). *J. Mol. Graph.* **15**, 132–134.
Hall, A. (1998). *Science*, **279**, 509–514.
Hirshberg, M., Stockley, R. W., Dodson, G. & Webb, M. R. (1997). *Nature Struct. Biol.* **4**, 147–152.
Hoffman, G. R., Nassar, N. & Cerione, R. A. (2000). *Cell*, **100**, 345–356.
Ihara, K., Muraguchi, S., Kato, M., Shimizu, T., Shirakawa, M., Kuroda, S., Kaibuchi, K. & Hakoshima, T. (1998). *J. Biol. Chem.* **273**, 9656–9666.
Jones, T. A., Zou, J. Y., Cowan, S. W. & Kjeldgaard, M. (1991). *Acta Cryst.* A**47**, 110–119.
Krengel, U., Schlichting, L., Scherer, A., Schumann, R., Frech, M., John, J., Kabsch, W., Pai, E. F. & Wittinghofer, A. (1990). *Cell*, **62**, 539–548.
Longenecker, K., Read, P., Derewenda, U., Dauter, Z., Liu, X., Garrard, S., Walker, L., Somlyo, A. V., Nakamoto, R. K., Somlyo, A. P. & Derewenda, Z. S. (1999). *Acta Cryst.* D**55**, 1503–1515.
Mayer, T., Meyer, M., Janning, A., Schiedel, A. C. & Barnekow, A. (1999). *Oncogene*, **18**, 2117–2128.
Michaelson, D., Silletti, J., Murphy, G., D'Eustachio, P., Rush, M. & Philips, M. R. (2001). *J. Cell Biol.* **152**, 111–126.
Murshudov, G. N., Vagin, A. A. & Dodson, E. J. (1997). *Acta Cryst.* D**53**, 240–255.
Nassar, N., Hoffman, G. R., Manor, D., Clardy, J. C. & Cerione, R. A. (1998). *Nature Struct. Biol.* **5**, 1047–1052.
Otwinowski, Z. & Minor, W. (1997). *Methods Enzymol.* **276**, 307–326.
Perrakis, A., Harkiolaki, M., Wilson, K. S. & Lamzin, V. S. (2001). *Acta Cryst.* D**57**, 1445–1450.
Read, P. W., Liu, X., Longenecker, K., DiPierro, C. G., Walker, L. A., Somlyo, A. V., Somlyo, A. P. & Nakamoto, R. K. (2000). *Protein Sci.* **9**, 376–386.
Read, P. W. & Nakamoto, R. K. (2000). *Methods Enzymol.* **325**, 15–25.
Rudolph, M. G., Wittinghofer, A. & Vetter, I. R. (1999). *Protein Sci.* **8**, 778–787.
Scheffzek, K., Stephan, I., Jensen, O. N., Illenberger, D. & Gierschik, P. (2000). *Nature Struct. Biol.* **7**, 122–126.
Sheffield, P., Garrard, S. & Derewenda, Z. (1999). *Protein Expr. Purif.* **15**, 34–39.
Somlyo, A. P. & Somlyo, A. V. (2000). *J. Physiol. (London)*, **522**, 177–185.
Tarricone, C., Xiao, B., Justin, N., Walker, P. A., Rittinger, K., Gamblin, S. J. & Smerdon, S. J. (2001). *Nature (London)*, **411**, 215–219.
Wei, Y., Zhang, Y., Derewenda, U., Liu, X., Minor, W., Nakamoto, R. K., Somlyo, A. V., Somlyo, A. P. & Derewenda, Z. S. (1997). *Nature Struct. Biol.* **4**, 699–703.
Winn, M. D., Isupov, M. N. & Murshudov, G. N. (2001). *Acta Cryst.* D**57**, 122–133.
Zohn, I. M., Campbell, S. L., Khosravi-Far, R., Rossman, K. L. & Der, C. J. (1998). *Oncogene*, **17**, 1415–1438.